

# Exact Spike Train Inference Via $\ell_0$ Optimization

Sean Jewell

*Department of Statistics  
University of Washington  
Seattle, Washington 98195  
e-mail: [swjewell@uw.edu](mailto:swjewell@uw.edu)*

Daniela Witten

*Departments of Biostatistics and Statistics  
University of Washington  
Seattle, Washington 98195  
e-mail: [dwitten@uw.edu](mailto:dwitten@uw.edu)*

**Abstract:** In recent years, new technologies in neuroscience have made it possible to measure the activities of large numbers of neurons in behaving animals. For each neuron, a *fluorescence trace* is measured; this can be seen as a first-order approximation of the neuron’s activity over time. Determining the exact time at which a neuron spikes on the basis of its fluorescence trace is an important open problem in the field of computational neuroscience.

Recently, a convex optimization problem involving an  $\ell_1$  penalty was proposed for this task. In this paper, we slightly modify that recent proposal by replacing the  $\ell_1$  penalty with an  $\ell_0$  penalty. In stark contrast to the conventional wisdom that  $\ell_0$  optimization problems are computationally intractable, we show that the resulting optimization problem can be efficiently solved for the global optimum using an extremely simple and efficient dynamic programming algorithm. Our R-language implementation of the proposed algorithm runs in a few minutes on fluorescence traces of 100,000 timesteps. Furthermore, our proposal leads to substantially better results than the previous  $\ell_1$  proposal, on synthetic data as well as on two calcium imaging data sets.

R-language software for our proposal is available on CRAN in the package `LZeroSpikeInference`.

## 1. Introduction

When a neuron spikes, calcium floods the cell. In order to quantify intracellular calcium levels, calcium imaging techniques make use of fluorescent calcium indicator molecules (Dombeck et al., 2007; Ahrens et al., 2013; Prevedel et al., 2014). Thus, a neuron’s *fluorescence trace* can be seen as a first-order approximation of its activity level over time.

However, the fluorescence trace itself is typically not of primary scientific interest: instead, it is of interest to determine the underlying neural activity, that is, the specific times at which the neuron spiked. Inferring the spike times on the basis of a fluorescence trace amounts to a challenging deconvolution problem, which has been the focus of substantial investigation (Grewe et al., 2010; Pnevmatikakis et al., 2013; Theis et al., 2016; Deneux et al., 2016;

Sasaki et al., 2008; Vogelstein et al., 2009; Yaksi and Friedrich, 2006; Vogelstein et al., 2010; Holekamp, Turaga and Holy, 2008; Friedrich and Paninski, 2016; Friedrich, Zhou and Paninski, 2017). In this paper, we propose a new approach for this task. Our approach is based upon a simple insight: an auto-regressive model for calcium dynamics considered by Friedrich and Paninski (2016) and Friedrich, Zhou and Paninski (2017) leads directly to a simple  $\ell_0$  optimization problem, for which an efficient and exact algorithm is available.

### 1.1. An Auto-Regressive Model for Calcium Dynamics

In this paper, we will consider an auto-regressive model for calcium dynamics recently proposed by Friedrich and Paninski (2016) and Friedrich, Zhou and Paninski (2017); this is closely related to models considered by Vogelstein et al. (2010) and Pnevmatikakis et al. (2016). To begin, we review the model. Let  $y_t$  denote the observed fluorescence at the  $t$ th timestep, and let  $c_t$  denote the unobserved underlying calcium concentration at the  $t$ th timestep. Consider approximating the calcium concentration dynamics with an auto-regressive model of order  $p$ , where  $p$  is a small positive integer, as follows:

$$\begin{aligned} y_t &= \beta_0 + \beta_1 c_t + \epsilon_t, & t = 1, \dots, T; \\ c_t &= \sum_{i=1}^p \gamma_i c_{t-i} + s_t, & t = p+1, \dots, T. \end{aligned} \quad (1)$$

In (1),  $s_t$  represents the effect of a neuron spike on the calcium concentration at the  $t$ th timestep, and  $\epsilon_t \sim (0, \sigma^2)$  represents a noise term. The quantities  $\gamma_1, \dots, \gamma_p$  are the parameters in the auto-regressive model. The quantity  $y_t$  is observed; all other quantities in (1) are unobserved. The parameter of interest is  $s_t$ : in particular, we would like to know whether a given element of  $s_t$  is non-zero, since that indicates whether the neuron spikes at the  $t$ th timestep.

In what follows, for ease of exposition, we assume  $\beta_0 = 0$  and  $\beta_1 = 1$  in (1); all results in this paper allow for general  $\beta_0$  and  $\beta_1$ . See Section 5 for additional details.

Then, rearranging terms, (1) becomes

$$\begin{aligned} y_t &= c_t + \epsilon_t, & t = 1, \dots, T; \\ s_t &= c_t - \sum_{i=1}^p \gamma_i c_{t-i}, & t = p+1, \dots, T. \end{aligned} \quad (2)$$

We now make the assumption that  $s_t$  is sparse, in the sense that at most timesteps there are no spikes. Consequently, for most values of  $t$ ,  $s_t \equiv c_t - \sum_{i=1}^p \gamma_i c_{t-i} = 0$ . Furthermore,  $s_t$  should be nonnegative, because the occurrence of a spike can lead to an increase, but never a decrease, in the calcium concentration. In the case of a first-order auto-regressive model ( $p = 1$ ), this leads naturally to the optimization problem

$$\underset{c_1, \dots, c_T, s_2, \dots, s_T}{\text{minimize}} \left\{ \frac{1}{2} \sum_{t=1}^T (y_t - c_t)^2 + \lambda \sum_{t=2}^T 1_{(s_t \neq 0)} \right\} \text{ subject to } s_t = c_t - \gamma c_{t-1} \geq 0, \quad (3)$$

where  $1_{(A)}$  is an indicator variable that equals 1 if the event  $A$  holds, and 0 otherwise. In (3),  $\lambda$  is a non-negative tuning parameter that controls the number of timesteps at which a spike occurs.

Unfortunately, the optimization problem (3) is highly non-convex, due to the presence of the indicator variable. In the statistics literature, this term is known as an  $\ell_0$  penalty. It is well-known that optimization involving  $\ell_0$  penalties is typically computationally intractable: in general, no efficient algorithms are available to solve for the global optimum.

Therefore, in light of the computational challenges associated with the  $\ell_0$  penalty in (3), the intractable  $\ell_0$  penalty can be replaced with a convex  $\ell_1$ , or *lasso* (Tibshirani, 1996), penalty which leads to the optimization problem

$$\underset{c_1, \dots, c_T, s_2, \dots, s_T}{\text{minimize}} \left\{ \frac{1}{2} \sum_{t=1}^T (y_t - c_t)^2 + \lambda \sum_{t=2}^T |s_t| \right\} \text{ subject to } s_t = c_t - \gamma c_{t-1} \geq 0. \quad (4)$$

The optimization problem (4) provides a decent approximation to the  $\ell_0$  problem (3): when the tuning parameter  $\lambda$  is large, then  $s_t$  is encouraged to equal zero, so that a small number of spikes are estimated. Friedrich and Paninski (2016) and Friedrich, Zhou and Paninski (2017) consider a slight modification to (4) by including an additional  $\ell_1$  penalty for the initial calcium concentration

$$\underset{c_1, \dots, c_T, s_2, \dots, s_T}{\text{minimize}} \left\{ \frac{1}{2} \sum_{t=1}^T (y_t - c_t)^2 + \lambda |c_1| + \lambda \sum_{t=2}^T |s_t| \right\} \text{ subject to } s_t = c_t - \gamma c_{t-1} \geq 0. \quad (5)$$

Most importantly, (4) and (5) are convex optimization problems, for which a well-developed set of optimization algorithms is available (Boyd and Vandenberghe, 2004; Hastie, Tibshirani and Friedman, 2009; Hastie, Tibshirani and Wainwright, 2015; Bien and Witten, 2016). In their paper, Friedrich and Paninski (2016) develop a very fast exact algorithm for solving the problem (5), and Friedrich, Zhou and Paninski (2017) develop an algorithm for solving the extension of (5) to the case of  $p > 1$ .

## 1.2. Contribution of This Paper

We reiterate here that the model of interest is (2). When  $p = 1$ , this model leads directly to the  $\ell_0$  optimization problem (3). In other words, under the model (2), (3) is the “right” optimization problem to be solving. (In fact, Friedrich, Zhou and Paninski (2017) allude to this in the “Hard shrinkage and  $\ell_0$  penalty” section of their paper.) However, in the interest of being able to develop an efficient algorithm, Friedrich and Paninski (2016) and Friedrich, Zhou and Paninski (2017) instead solve the  $\ell_1$  problem (5). Other approximations to the  $\ell_0$  penalty have been used for similar deconvolution problems (de Rooi and Eilers, 2011; de Rooi, Ruckebusch and Eilers, 2014; Hugelier et al., 2016).

However, using an  $\ell_1$  norm to approximate an  $\ell_0$  norm comes with computational advantages at the expense of performance disadvantages: in particular, the use of an  $\ell_1$  penalty tends to *overshrink* the fitted estimates (Zou, 2006). It can be seen quite clearly in Figure 1 that the  $\ell_1$  problem (5) does indeed overshrink the fitted estimates.

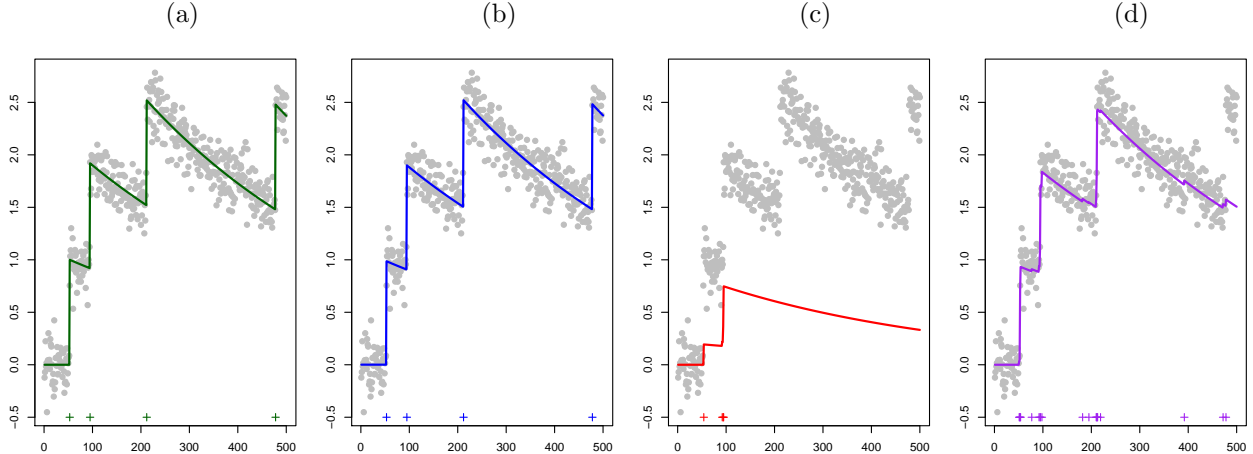


Fig 1: A toy simulated data example. In each panel, the  $x$ -axis represents time. Observed fluorescence values are displayed in ( $\bullet$ ). (a): Unobserved calcium concentrations ( $—$ ) and true spike times ( $+$ ). (b): Estimated calcium concentrations ( $—$ ) and spike times ( $+$ ) that result from solving the  $\ell_0$  optimization problem (6). (c): Estimated calcium concentrations ( $—$ ) and spike times ( $+$ ) that result from solving the  $\ell_1$  optimization problem (5) with the value of  $\lambda$  that yields the true number of spikes. This value of  $\lambda$  leads to very poor estimation of both the underlying calcium dynamics and the spikes. (d): Estimated calcium concentrations ( $—$ ) and spike times ( $+$ ) that result from solving the  $\ell_1$  optimization problem (5) with the largest value of  $\lambda$  that results in at least one estimated spike within the vicinity of each true spike. This value of  $\lambda$  results in 19 estimated spikes, which is far more than the true number of spikes. The poor performance of the  $\ell_1$  optimization problem in panels (c) and (d) is a consequence of the fact that the  $\ell_1$  penalty performs shrinkage as well as spike estimation; this is discussed further in Section 1.2.

In this paper, we consider a slight modification of (3) that results from removing the positivity constraint,

$$\underset{c_1, \dots, c_T, s_2, \dots, s_T}{\text{minimize}} \left\{ \frac{1}{2} \sum_{t=1}^T (y_t - c_t)^2 + \lambda \sum_{t=2}^T 1_{(s_t \neq 0)} \right\} \text{ subject to } s_t = c_t - \gamma c_{t-1}. \quad (6)$$

In practice, the distinction between the problems (6) and (3) is quite minor: for the most part on data applications, the solution to (6) tends to satisfy the constraint in (3), and so the solutions are identical.

Like problem (3), solving problem (6) for the global optimum appears, at a glance, to be computationally intractable — we (the authors) are only aware of a few  $\ell_0$  optimization problems for which exact solutions can be obtained via efficient algorithms!

However, in this paper, we show that in fact, (6) is a rare  $\ell_0$  optimization problem that can be *exactly solved for the global optimum using an efficient algorithm*. This is because (6) can be seen as a changepoint detection problem, for which efficient algorithms that run in no more than  $\mathcal{O}(T^2)$  time, and often closer to  $\mathcal{O}(T)$  time, are available. Furthermore, our implementation of the exact algorithm for solving (6) yields excellent results relative to the

convex approximation (5) considered by Friedrich and Paninski (2016) and Friedrich, Zhou and Paninski (2017). This vastly improved performance can be seen in Figure 1(b).

The rest of this paper is organized as follows. In Section 2, we present an exact algorithm for solving the  $\ell_0$  problem (6). In Section 3, we investigate the performance of this algorithm, relative to the algorithm of Friedrich and Paninski (2016) and Friedrich, Zhou and Paninski (2017) for solving the  $\ell_1$  problem (5), in a simulation study. In Section 4, we investigate the performances of both algorithms for spike train inference on a data set for which the true spike times are known (Chen et al., 2013; GENIE Project, 2015) and on a data set from the Allen Brain Observatory (Allen Institute for Brain Sciences, 2016; Hawrylycz et al., 2016). In Section 5 we generalize the problem (6), in order to allow for efficient estimation of an intercept term, to accommodate an auto-regressive model of order  $p > 1$  (1), and for more sophisticated calcium dynamics between spikes. Finally, we close with a discussion in Section 6. Technical details, as well as a comparison to heuristic approaches for improving upon the solution to (5), are provided in the Appendix.

## 2. An Exact Algorithm for Solving Problem (6)

In Section 2.1, we show that problem (6) can be viewed as a changepoint detection problem. In Sections 2.2 and 2.3, we apply existing algorithms for changepoint detection in order to efficiently solve (6) for the global optimum in  $\mathcal{O}(T^2)$  and in approximately  $\mathcal{O}(T)$  operations, respectively. Timing results are presented in Section 2.4. A modified cross-validation scheme for selecting the tuning parameter  $\lambda$  and auto-regressive parameter  $\gamma$  in (6) is discussed in Appendix B.

### 2.1. Recasting (6) as a Changepoint Detection Problem

Recall that our goal is to solve the  $\ell_0$  optimization problem (6), or equivalently, to compute  $\hat{c}_1, \dots, \hat{c}_T$  that solve the optimization problem

$$\text{minimize}_{c_1, \dots, c_T} \left\{ \frac{1}{2} \sum_{t=1}^T (y_t - c_t)^2 + \lambda \sum_{t=2}^T 1_{(c_t - \gamma c_{t-1} \neq 0)} \right\}.$$

We estimate a spike at the  $t$ th timestep if  $\hat{c}_t \neq \gamma \hat{c}_{t-1}$ . We now make two observations about this optimization problem.

1. Given that a spike is estimated at the  $t$ th timestep, the estimated calcium concentration at any time  $t_1 < t$  is independent of the estimated calcium concentration at any time  $t_2 \geq t$ .
2. Given that two spikes are estimated at the  $t$ th and  $t'$ th timesteps with  $t < t'$ , and no spikes are estimated in between the  $t$ th and  $t'$ th timesteps, the calcium concentration is estimated to decay exponentially between the  $t$ th and  $t'$ th timesteps.

This motivates us to consider the relationship between (6) and a *changepoint detection problem* (Aue and Horváth, 2013; Braun and Muller, 1998; Davis, Lee and Rodriguez-Yam, 2006;

Yao, 1988; Lee, 1995; Jackson et al., 2005; Killick, Fearnhead and Eckley, 2012; Maidstone et al., 2016) of the form

$$\underset{0=\tau_0<\tau_1<\dots<\tau_k<\tau_{k+1}=T, k}{\text{minimize}} \left\{ \sum_{j=0}^k \mathcal{D}(y_{(\tau_j+1):\tau_{j+1}}) + \lambda k \right\}, \quad (7)$$

where

$$\mathcal{D}(y_{a:b}) \equiv \min_{c_t=\gamma c_{t-1}, t=a+1, \dots, b} \left\{ \frac{1}{2} \sum_{t=a}^b (y_t - c_t)^2 \right\}. \quad (8)$$

In (7), we are simultaneously minimizing the objective over the times at which the change-points  $(\tau_1, \dots, \tau_k)$  occur and the number of changepoints  $(k)$ ; the parameter  $\lambda$  controls the relative importance of these two terms.

The following result establishes an equivalence between (7) and (6).

**Proposition 1** *There is a one-to-one correspondence between the set of estimated spikes in the solution to (6) and the set of changepoints  $0 = \tau_0, \tau_1, \dots, \tau_k, \tau_{k+1} = T$  in the solution to (7), in the sense that  $\hat{c}_t \neq \gamma \hat{c}_{t-1}$  if and only if  $t \in \{\tau_1 + 1, \dots, \tau_k + 1\}$ . Furthermore, given the set of changepoints, the solution to (6) takes the form*

$$\hat{c}_t = \begin{cases} \gamma \hat{c}_{t-1} & \tau_j + 2 \leq t \leq \tau_{j+1} \\ \frac{\sum_{t=\tau_j+1}^{\tau_{j+1}} y_t \gamma^{t-(\tau_j+1)}}{\sum_{t=\tau_j+1}^{\tau_{j+1}} \gamma^{2(t-(\tau_j+1))}} & t = \tau_j + 1 \end{cases},$$

for  $j \in \{0, \dots, k\}$ .

Proposition 1 indicates that in order to solve (6), it suffices to solve (7). (We note that due to a slight discrepancy between the conventions used in the changepoint detection literature and the notion of a spike in this paper, the indexing in Proposition 1 is a little bit awkward, in the sense that the  $k$ th spike is estimated to occur at time  $\tau_k + 1$ , rather than at time  $\tau_k$ .)

In the next two sections, we will make use of the following result.

**Proposition 2** *The quantity (8) has a closed-form expression,*

$$\mathcal{D}(y_{a:b}) = \sum_{t=a}^b \frac{y_t^2}{2} - \mathcal{C}(y_{a:b}) \sum_{t=a}^b y_t \gamma^{t-a} + \frac{\mathcal{C}(y_{a:b})^2}{2} \sum_{t=a}^b \gamma^{2(t-a)}, \text{ where}$$

$$\mathcal{C}(y_{a:b}) = \frac{\sum_{t=a}^b y_t \gamma^{t-a}}{\sum_{t=a}^b \gamma^{2(t-a)}}.$$

Furthermore, given  $\mathcal{D}(y_{a:b})$ , we can calculate  $\mathcal{D}(y_{a:(b+1)})$  in constant time.

Propositions 1 and 2 are proven in Appendix A.

## 2.2. An Algorithm for Solving (6) in $\mathcal{O}(T^2)$ Operations

In this section, we apply a dynamic programming algorithm proposed by Jackson et al. (2005) and Auger and Lawrence (1989) in order to solve the changepoint detection problem (7) for

the global optimum in  $\mathcal{O}(T^2)$  time. Due to the equivalence between (7) and (6) established in Proposition 1, this algorithm also solves problem (6).

Roughly speaking, this algorithm recasts the very difficult problem of choosing the times of all changepoints simultaneously into the much simpler problem of choosing the time of just the most recent changepoint. In greater detail, consider solving (7) on the first  $s$  timesteps. Define  $F(0) \equiv -\lambda$ , and for  $s \geq 1$ , define

$$\begin{aligned}
F(s) &= \min_{0=\tau_0 < \tau_1 < \dots < \tau_k < \tau_{k+1}=s, k} \left\{ \sum_{j=0}^k \mathcal{D}(y_{(\tau_j+1):\tau_{j+1}}) + \lambda k \right\} \\
&= \min_{0=\tau_0 < \tau_1 < \dots < \tau_k < \tau_{k+1}=s, k} \left\{ \sum_{j=0}^k [\mathcal{D}(y_{(\tau_j+1):\tau_{j+1}}) + \lambda] - \lambda \right\} \\
&= \min_{0=\tau_0 < \tau_1 < \dots < \tau_k < \tau_{k+1}=s, k} \left\{ \sum_{j=0}^{k-1} [\mathcal{D}(y_{(\tau_j+1):\tau_{j+1}}) + \lambda] - \lambda + \mathcal{D}(y_{(\tau_k+1):\tau_{k+1}}) + \lambda \right\} \\
&= \min_{0 \leq \tau_k < \tau_{k+1}=s} \left\{ \min_{0=\tau_0 < \tau_1 < \dots < \tau_{k'} < \tau_{k'+1}=\tau_k, k'} \left\{ \sum_{j=0}^{k'} [\mathcal{D}(y_{(\tau_j+1):\tau_{j+1}}) + \lambda] - \lambda \right\} + \mathcal{D}(y_{(\tau_k+1):\tau_{k+1}}) + \lambda \right\} \\
&= \min_{0 \leq \tau < s} \left\{ F(\tau) + \mathcal{D}(y_{(\tau+1):s}) + \lambda \right\}. \tag{9}
\end{aligned}$$

In other words, in order to solve (7), we need simply identify the time of the most recent changepoint, and then solve (7) on all earlier times.

This recursion gives a simple recipe for evaluating  $F(T)$  efficiently: set  $F(0) = -\lambda$ , and compute  $F(1), F(2), \dots, F(T)$  based on previously calculated (and stored) values. For example, at  $s = 1$ , calculate and store

$$F(1) = \min_{0 \leq \tau < 1} \left\{ F(\tau) + \mathcal{D}(y_{(\tau+1):1}) + \lambda \right\} = F(0) + \mathcal{D}(y_1) + \lambda,$$

and then at  $s = 2$  use the previously calculated values  $F(0)$  and  $F(1)$  to compute the minimum over a finite set with  $s$  elements

$$F(2) = \min_{\tau \in \{0,1\}} \left\{ F(\tau) + \mathcal{D}(y_{(\tau+1):2}) + \lambda \right\} = \min \{ F(0) + \mathcal{D}(y_{1:2}) + \lambda, F(1) + \mathcal{D}(y_2) + \lambda \}.$$

Given  $F(1), \dots, F(s-1)$ , computing  $F(s)$  requires minimizing over a finite set of size  $s$ , and therefore it has computational cost linear in  $s$ . The total cost of computing  $F(T)$  is quadratic in the total number of timesteps,  $T$ , since there are  $T+1$  subproblems:  $\sum_{s=0}^T s = \mathcal{O}(T^2)$ .

Full details are provided in Algorithm 1. We note that this algorithm is particularly efficient in light of Proposition 2, which makes it possible to perform a constant-time update to  $\mathcal{D}(y_{(\tau+1):s})$  in order to compute  $\mathcal{D}(y_{(\tau+1):(s+1)})$ .

### 2.3. An Algorithm for Solving (6) in Approximately $\mathcal{O}(T)$ Operations

In a recent paper, [Killick, Fearnhead and Eckley \(2012\)](#) considered problems of the form (7) for which an assumption on  $\mathcal{D}(\cdot)$  holds; this assumption is satisfied by (8).

---

**Algorithm 1:** An  $\mathcal{O}(T^2)$  Algorithm for Solving (6)

---

**Initialize:**  $F(0) = -\lambda$ ,  $cp(0) = \emptyset$   
1 **foreach**  $s = 1, 2, \dots, T$  **do**  
2     Calculate  $F(s) = \min_{0 \leq \tau < s} \{F(\tau) + \mathcal{D}(y_{(\tau+1):s}) + \lambda\}$   
3     Set  $s' = \operatorname{argmin}_{0 \leq \tau < s} \{F(\tau) + \mathcal{D}(y_{(\tau+1):s}) + \lambda\}$   
4     Update  $cp(s) = (cp(s'), s')$   
5 **end**  
**Output :** The number of spikes  $k \equiv \operatorname{card}(cp(T))$ , the changepoints  $\{\tau_1, \dots, \tau_k\} \equiv cp(T)$ , the spike times  $\{\tau_1 + 1, \dots, \tau_k + 1\}$ , and the estimated calcium concentrations

$$\hat{c}_t \equiv \begin{cases} \gamma \hat{c}_{t-1} & \tau_j + 2 \leq t \leq \tau_{j+1} \\ \frac{\sum_{t=\tau_j+1}^{\tau_{j+1}} y_t \gamma^{t-(\tau_j+1)}}{\sum_{t=\tau_j+1}^{\tau_{j+1}} \gamma^{2(t-(\tau_j+1))}} & t = \tau_j + 1 \end{cases},$$

for  $j = 0, \dots, k$ , where  $\tau_0 = 0$ .

---

The main insight of their paper is as follows. Suppose that  $s < r$  and  $F(s) + \mathcal{D}(y_{(s+1):r}) > F(r)$ . Then for any  $q > r$ , it is mathematically impossible for the most recent changepoint before the  $q$ th timestep to have occurred at the  $s$ th timestep. This allows us to *prune* the set of candidate changepoints that must be considered in each step of Algorithm 2, leading to drastic speed-ups.

Details are provided in Algorithm 2, which solves (6) for the global optimum.

Under several technical assumptions, Killick, Fearnhead and Eckley (2012) show that the expected complexity of this algorithm is  $\mathcal{O}(T)$ . The main assumption is that the expected number of changepoints in the data increases linearly with the length of the data; this is reasonable in the context of calcium imaging data, in which we expect the number of neuron spikes to be linear in the length of the recording.

---

**Algorithm 2:** An  $\mathcal{O}(T)$  Algorithm for Solving (6)

---

**Initialize:**  $F(0) = -\lambda$ ,  $cp(0) = \emptyset$ ,  $\mathcal{E}_1 = \{0\}$   
1 **foreach**  $s = 1, 2, \dots, T$  **do**  
2     Calculate  $F(s) = \min_{\tau \in \mathcal{E}_s} \{F(\tau) + \mathcal{D}(y_{(\tau+1):s}) + \lambda\}$   
3     Set  $s' = \operatorname{argmin}_{\tau \in \mathcal{E}_s} \{F(\tau) + \mathcal{D}(y_{(\tau+1):s}) + \lambda\}$   
4     Update  $\mathcal{E}_{s+1} = \{\tau \in \{\mathcal{E}_s \cup s\} : F(\tau) + \mathcal{D}(y_{(\tau+1):s}) < F(s)\}$   
5     Update  $cp(s) = (cp(s'), s')$   
6 **end**  
**Output :** The number of spikes  $k \equiv \operatorname{card}(cp(T))$ , the changepoints  $\{\tau_1, \dots, \tau_k\} \equiv cp(T)$ , the spike times  $\{\tau_1 + 1, \dots, \tau_k + 1\}$ , and the estimated calcium concentrations

$$\hat{c}_t \equiv \begin{cases} \gamma \hat{c}_{t-1} & \tau_j + 2 \leq t \leq \tau_{j+1} \\ \frac{\sum_{t=\tau_j+1}^{\tau_{j+1}} y_t \gamma^{t-(\tau_j+1)}}{\sum_{t=\tau_j+1}^{\tau_{j+1}} \gamma^{2(t-(\tau_j+1))}} & t = \tau_j + 1 \end{cases},$$

for  $j = 0, \dots, k$ , where  $\tau_0 = 0$ .

---

## 2.4. Timing Results for Solving (6)

We simulated data from (1) with  $p = 1$ ,  $\gamma = 0.998$ ,  $\sigma = 0.15$ , and  $s_t \sim_{\text{i.i.d.}} \text{Poisson}(0.009)$ . We solved (6) with  $\lambda = 1$ , using our R-language implementations of Algorithms 1 and 2.

Timing results, averaged over 50 simulated data sets, are displayed in Figure 2. As expected, the running time of Algorithm 1 scales quadratically in the length of the time series, whereas Algorithm 2 scales approximately linearly. Using Algorithm 2, we can solve (6) for the global optimum on fluorescence traces of length 100,000 in a few minutes on a 2.5 GHz Intel Core i7 Macbook Pro.

We note here that Algorithm 2 for solving (6) is much slower than the algorithm of Friedrich, Zhou and Paninski (2017) for solving (5), which is implemented in Cython and has approximate linear running time. It should be possible to develop a faster algorithm for solving (6) using ideas from Johnson (2013) and Maidstone et al. (2016). Furthermore, a much faster implementation of Algorithm 2 would be possible using a language other than R. However, we leave such improvements to future work, given that our current implementation of Algorithm 2 is fast enough to conveniently run on large-scale data sets.

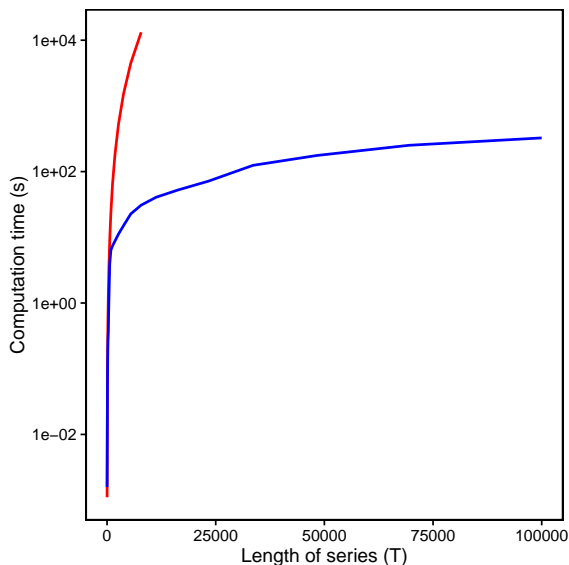


Fig 2: Timing results for solving (6) for the global optimum, using Algorithms 1 (—) and 2 (—). The  $x$ -axis displays the length of the time series ( $T$ ), and the  $y$ -axis displays the average running time, in seconds. Additional details are provided in Section 2.4.

## 3. Simulation Study

In this section, we use *in silico* data to demonstrate the performance advantages of the  $\ell_0$  approach (6) over the  $\ell_1$  proposal (5) of Friedrich and Paninski (2016) and Friedrich, Zhou and Paninski (2017).

### 3.1. Performance Measures

We measure performance of each method based on two criteria: (i) error in calcium estimation, and (ii) error in spike detection.

We consider the mean of squared differences between the true calcium concentration in (1) and the estimated calcium concentration that solves (6),

$$\text{MSE}(c, \hat{c}) = \frac{1}{T} \sum_{t=1}^T (c_t - \hat{c}_t)^2. \quad (10)$$

This quantity involves the unobserved calcium concentrations,  $c_1, \dots, c_T$ , and thus can only be computed on simulated data.

We now consider the task of quantifying the error in spike detection. A number of measures of dissimilarity between sets of changepoints have been proposed in the literature (Boysen et al., 2009; Harchaoui and Lévy-Leduc, 2010). However, for the most part, these measures are somewhat unintuitive and do not account for the possibility of multiple true spikes at a single timestep.

Therefore, we take the following approach. Let  $z_t$  denote the number of true spikes at the  $t$ th timestep, and let  $\hat{z}_t$  denote the number of estimated spikes at the  $t$ th timestep. Let  $z$  and  $\hat{z}$  denote the  $T$ -vectors for which the  $t$ th elements are  $z_t$  and  $\hat{z}_t$ , respectively. In order to account for small differences in spike times that are not of practical importance, we smooth each vector with a Gaussian kernel: that is,  $r(z)$  and  $r(\hat{z})$  result from smoothing the vectors  $z$  and  $\hat{z}$  with a Gaussian kernel of bandwidth  $h = 5$ . Then, we define the distance between  $z$  and  $\hat{z}$  as

$$\text{dist}(z, \hat{z}) = \frac{1}{T} \sum_{t=1}^T (r(z)_t - r(\hat{z})_t)^2. \quad (11)$$

### 3.2. Results

We generated 50 simulated data sets according to (1) with  $p = 1$ , and parameter settings  $\gamma = 0.998$ ,  $T = 10000$ , and  $\sigma = 0.15$ . At each timestep,  $s_t \sim_{\text{i.i.d.}} \text{Pois}(0.005)$ . On each simulated data set, we solved (6) and (5) for a range of values of the tuning parameter  $\lambda$ .

Figure 3(a) displays the error in spike detection (11), and Figure 3(b) displays the error in calcium estimation (10), for the  $\ell_0$  problem (6) and for the  $\ell_1$  problem (5), for a range of values of  $\lambda$ . Results are averaged over the 50 simulated data sets. We note that due to the non-negativity constraint in (5), even for very small values of the tuning parameter  $\lambda$ , the solution contains no more than around 300 spikes on average. Consequently, the curves corresponding to (5) appear truncated in Figure 3.

First of all, we notice that solving the  $\ell_0$  problem (6) results in dramatically lower errors in both calcium estimation and spike detection than solving the  $\ell_1$  problem (5). Furthermore, the  $\ell_0$  problem (6) achieves the lowest errors in both calcium estimation and spike detection when applied using a value of the tuning parameter  $\lambda$  that yields approximately 50 estimated spikes, which is the expected number of spikes in this simulation. In fact, the cross-validation

approach for selecting  $\gamma$  and  $\lambda$  that is described in detail in Appendix B produces fits that on average have 46 spikes, and hence yields very good results in this simulation.

We see from Figure 3(a) that the  $\ell_1$  approach (5) achieves its lowest error in spike detection when we estimate approximately 50 spikes; recall that there are approximately 50 true spikes in this simulation. By contrast, in Figure 3(b), the  $\ell_1$  approach achieves its lowest error in calcium estimation when a much larger number of spikes is estimated. This is a consequence of the fact that the  $\ell_1$  penalty simultaneously controls both the number of estimated spikes well as the shrinkage of the estimated calcium. Therefore, the value of the tuning parameter  $\lambda$  in (5) that yields the most accurate estimate of calcium will result in severe over-estimation of the number of spikes. One immediate consequence of this phenomenon is that the cross-validation scheme detailed in Appendix B will not perform well for the  $\ell_1$  approach.

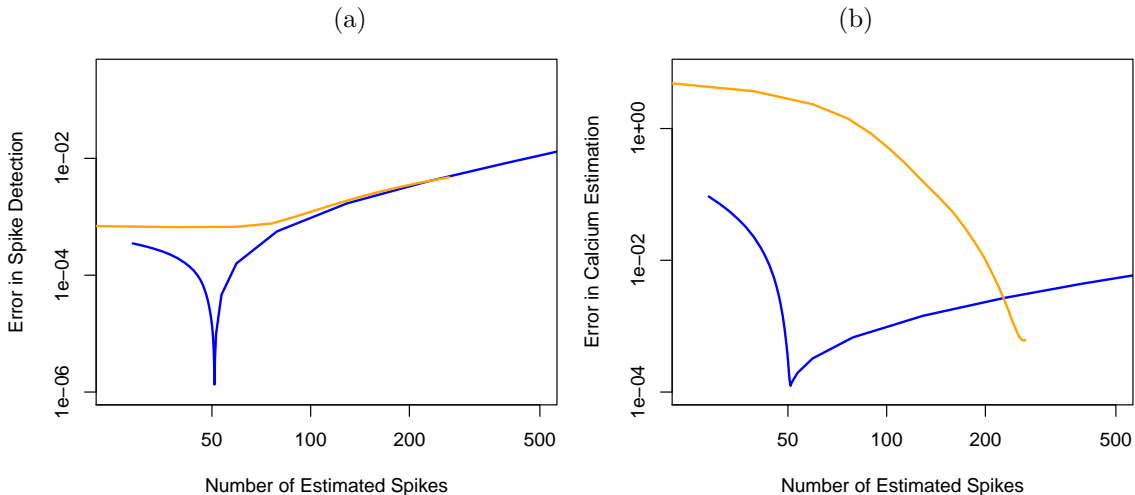


Fig 3: Simulation study to assess the error in spike detection and calcium estimation, for the  $\ell_1$  (—) and  $\ell_0$  (—) problems. (a): Error in spike detection (11). (b): Error in calcium estimation (10). Simulation details are provided in Section 3.

## 4. Application to Calcium Imaging Data

In this section, we apply our  $\ell_0$  proposal (6) and the  $\ell_1$  proposal of Friedrich and Paninski (2016) and Friedrich, Zhou and Paninski (2017) (5) to two calcium imaging data sets. In the first data set, the true spike times are known (Chen et al., 2013; GENIE Project, 2015), and so we can directly assess the spike detection accuracy of each proposal. In the second data set, the true spike times are unknown (Allen Institute for Brain Sciences, 2016; Hawrylycz et al., 2016); nonetheless, we are able to make a qualitative comparison of the results of the  $\ell_1$  and  $\ell_0$  proposals.

### 4.1. Application to Chen et al. (2013) Data

We first consider the data set of Chen et al. (2013) and GENIE Project (2015), which consists of simultaneous calcium imaging and electrophysiological measurements. This data

set was obtained from the Collaborative Research in Computational Neuroscience portal (<http://crcns.org/data-sets/methods/cai-1/about-cai-1>). In what follows, we refer to the spike times inferred from the electrophysiological measurements as the “true” spikes.

The top panel of Figure 4 shows a 40-second recording from cell 2002, which expresses GCaMP6s. The data are measured at 60 Hz, for a total of 2400 timesteps. The raw fluorescence traces are  $DF/F$  transformed with a 20% percentile filter as in Figure 3 of Friedrich, Zhou and Paninski (2017). In this 40-second recording, there are a total of 23 true spikes; therefore, we solved the  $\ell_0$  and  $\ell_1$  problems with  $\gamma = 0.9864405$  using values of  $\lambda$  in (6) and (5) that yield 23 estimated spikes.

Figure 4 displays the estimated spikes resulting from the  $\ell_0$  proposal, the estimated spikes resulting from the  $\ell_1$  proposal, and the ground truth spikes. We see that the  $\ell_0$  proposal has one false negative (i.e. it misses one true spike at around 7 seconds) and one false positive (i.e. it estimates a spike at around 36 seconds, where there is no true spike). By contrast, the  $\ell_1$  problem concentrates the 23 estimated spikes at three points in time, and therefore suffers from a substantial number of false positives as well as false negatives. Because the  $\ell_1$  penalty controls both the number of spikes and the estimated calcium, the  $\ell_1$  problem tends to put a large number of spikes in a row, each of which is associated with a very modest increase in calcium. This is consistent with the results seen in Figures 1 and 3.

In Appendix C, we consider two alternative approaches for analyzing this data: (i) we threshold the solution  $\hat{s}_2, \dots, \hat{s}_T$  of the  $\ell_1$  problem in order to further encourage sparsity by eliminating small spikes, and (ii) we apply an approach proposed by Friedrich, Zhou and Paninski (2017) to approximate the solution to a non-convex problem using a greedy algorithm. Both alternative approaches perform quite a bit better than solving the  $\ell_1$  problem (5). In particular, the latter approach performs pretty well in this example, though it does not achieve the global optimum.

#### 4.2. Application to Allen Brain Observatory Data

We now consider a data set from the Allen Brain Observatory, a large open-source repository of calcium imaging data from the mouse visual cortex (Allen Institute for Brain Sciences, 2016; Hawrylycz et al., 2016). For this data, the true spike times are not available, and so it is difficult to objectively assess the performances of the  $\ell_1$  and  $\ell_0$  methods. Instead, for each method we present several fits that differ in the number of detected spikes. We argue that the  $\ell_0$  problem yields results that are qualitatively superior to those of the  $\ell_1$  problem, in the sense that they better correspond to what we see from visual inspection of the data.

For the second ROI in NWB 510221121, we applied the  $\ell_1$  and  $\ell_0$  methods to the first 10,000 timesteps of the  $DF/F$ -transformed fluorescence traces. Since the data are measured at 30 Hz, this amounts to the first 333 seconds of the recording. Figure 5 shows the results obtained with  $\gamma = 0.981756$  when the tuning parameter  $\lambda$  was chosen in (5) and (6) to yield 27, 49, and 128 estimated spikes.

As in the previous subsection, we see that when faced with a large increase in fluorescence, the  $\ell_1$  problem tends to estimate a very large number of spikes in quick succession. For example, when 27 spikes are estimated, the  $\ell_1$  problem concentrates the estimated spikes at

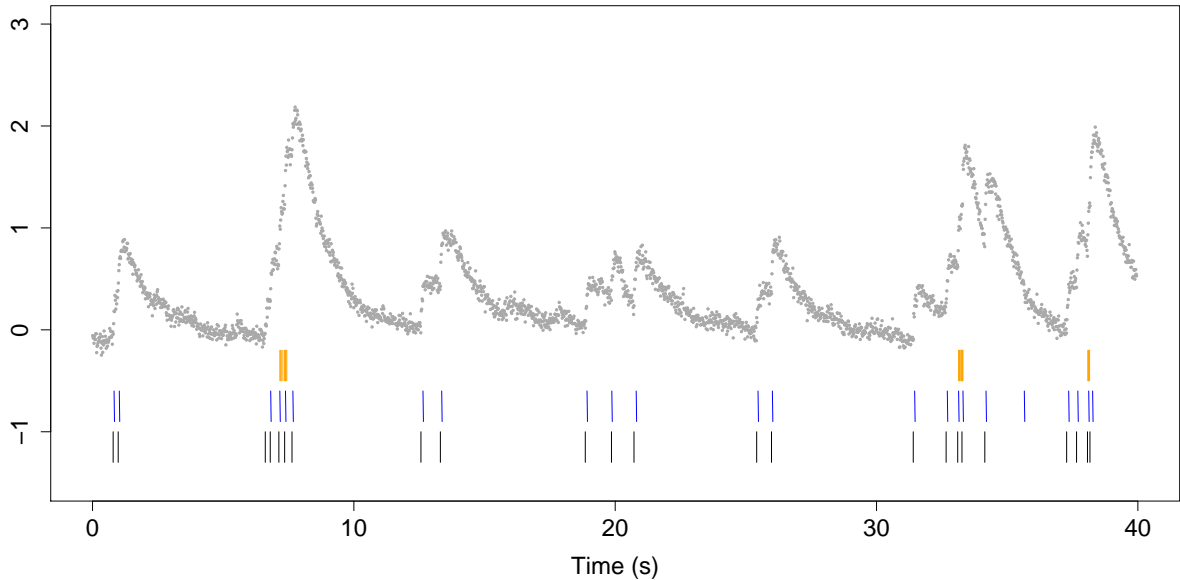


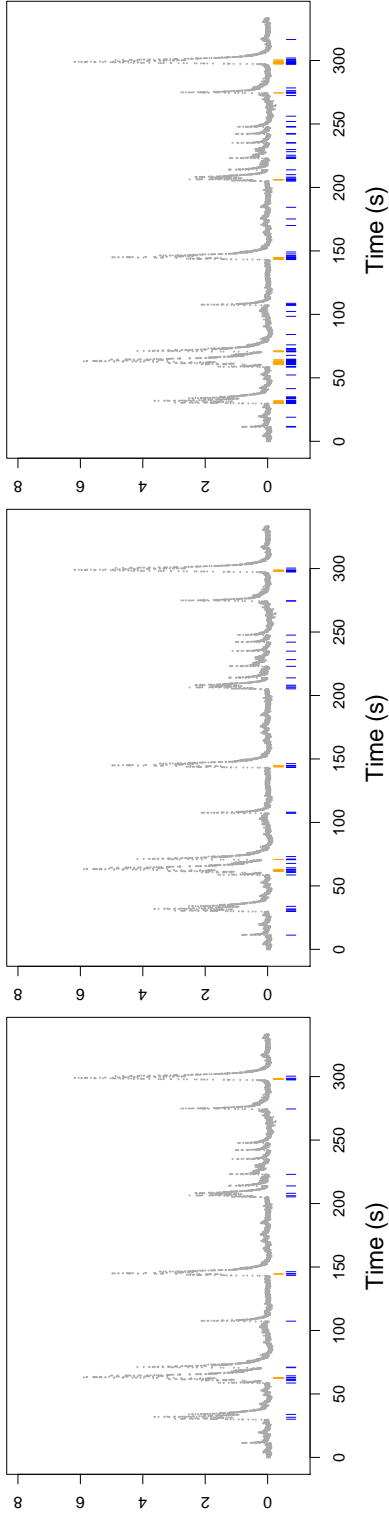
Fig 4: Spike detection for cell 2002 of the [Chen et al. \(2013\)](#) data. The observed fluorescence ( $\bullet$ ) and true spikes ( $—$ ) are displayed. Estimated spikes from the  $\ell_0$  problem are shown in ( $—$ ), and estimated spikes from the  $\ell_1$  problem (5) are shown in ( $—$ ).

three points in time (Figure 5(a)). Even when 128 spikes are estimated, the  $\ell_1$  problem still seems to miss all but the largest peaks in the fluorescence data (Figure 5(c)).

By contrast, the  $\ell_0$  problem can assign an arbitrarily large increase in calcium to a single spike. Therefore, it seems to capture most of the visible peaks in the fluorescence data when 49 spikes are estimated, and it captures all of them when 128 spikes are estimated (Figure 5(b)–(c)).

Additional insight into the results of the  $\ell_0$  and  $\ell_1$  proposals can be seen in Figures 5(d)–(f), which zoom in on a subset of the timesteps displayed in Figures 5(a)–(c). It is clear that the  $\ell_0$  method attempts to distribute the estimated spikes in order to accommodate all of the peaks in fluorescence, whereas the  $\ell_1$  method concentrates the estimated spikes around only the very largest fluorescence peaks.

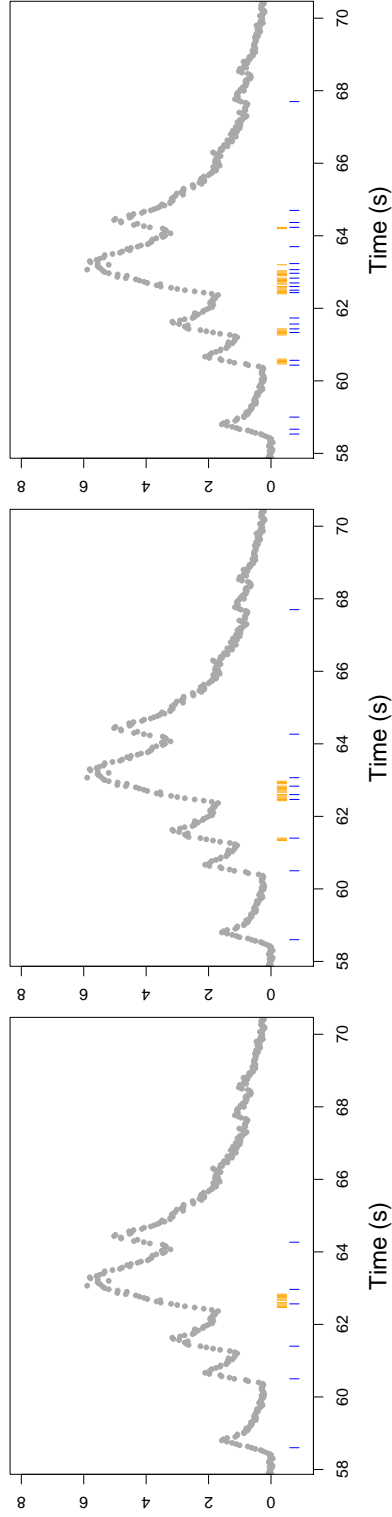
Though the true spike times are unknown for this data, based on visual inspection, the results for the  $\ell_0$  proposal seem superior to those of the  $\ell_1$  proposal.



(a) 27 spikes.

(b) 49 spikes.

(c) 128 spikes.



(d) Zoomed 27 spikes.

(e) Zoomed 49 spikes.

(f) Zoomed 128 spikes.

Fig 5: The first 10,000 timesteps from the second ROI in NWB 510221121 from the Allen Brain Observatory. Each panel displays the DF/F-transformed fluorescence ( $\bullet$ ), the estimated spikes from the  $\ell_0$  problem (—) (6), and the estimated spikes from the  $\ell_1$  problem (—) (5). The panels display results from applying the  $\ell_1$  and  $\ell_0$  methods with tuning parameter  $\lambda$  chosen to yield (a): 27 spikes for each method; (b): 49 spikes for each method; and (c): 128 spikes for each method. (d)–(f): As in (a)–(c), but zoomed in on 58–70 seconds.

## 5. Extensions

We now present three straightforward extensions to the optimization problem (6), for which computationally attractive algorithms along the lines of the one proposed in Section 2 are available.

### 5.1. Estimation of the Intercept in (1)

The model for calcium dynamics considered in this paper (1) allows for an intercept term,  $\beta_0$ . In order to arrive at (6), we assumed that the intercept was known and (without loss of generality) equal to zero. However, in practice, we might want to fit the model (1) without knowing the value of the intercept  $\beta_0$ . In fact, in many settings, this may be of great practical importance, since the meaning of the model (1) (and, for instance, the rate of exponential decay  $\gamma$ ) is inextricably tied to the value of the intercept.

We now propose a modification to the  $\ell_0$  optimization problem (6) that allows for estimation of the intercept  $\beta_0$ . So that the resulting problem can be efficiently solved using the ideas laid out in Section 2, we must ensure that given the estimated spike times, the calcium can be estimated separately between each pair of consecutive spikes. Consequently, we must allow for a separate intercept term between each pair of consecutive spikes. This suggests the optimization problem

$$\text{minimize}_{c_1, \dots, c_T, \beta_{01}, \dots, \beta_{0T}} \left\{ \frac{1}{2} \sum_{t=1}^T (y_t - c_t - \beta_{0t})^2 + \lambda \sum_{t=2}^T 1_{(c_t \neq \gamma c_{t-1}, \beta_{0t} \neq \beta_{0,t-1})} \right\}, \quad (12)$$

where the indicator variable  $1_{(A,B)}$  equals 1 if the event  $A \cup B$  holds, and equals zero otherwise. Therefore,  $1_{(c_t \neq \gamma c_{t-1}, \beta_{0t} \neq \beta_{0,t-1})}$  equals 1 if the calcium concentration stops decaying or if the intercept changes. Note that in the solution to (12), the intercept is constant between any pair of consecutive spikes, but may take on different values between two different pairs of spikes.

Problem (12) can be recast as a changepoint problem of the form (7) with

$$\mathcal{D}(y_{a:b}) \equiv \min \left\{ \frac{1}{2} \sum_{t=a}^b (y_t - c_t - \beta_{0t})^2 \right\} \text{ subject to } c_t = \gamma c_{t-1}, \beta_{0t} = \beta_{0,t-1}, \quad t = a + 1, \dots, b.$$

Given  $\mathcal{D}(y_{a:b})$ ,  $\mathcal{D}(y_{a:(b+1)})$  can be updated in constant time. Thus, the algorithms introduced in Section 2 can be easily modified in order to solve (12) for the global optimum.

### 5.2. An Auto-Regressive Model with $p > 1$ in (1)

The model (1) allows for the calcium dynamics to follow a  $p$ th order auto-regressive process. For simplicity, this paper focused on the case of  $p = 1$ . We now consider developing an  $\ell_0$  optimization problem for the model (1) with  $p > 1$ .

It is natural to consider the  $\ell_0$  optimization problem

$$\text{minimize}_{c_1, \dots, c_T} \left\{ \frac{1}{2} \sum_{t=1}^T (y_t - c_t)^2 + \lambda \sum_{t=p+1}^T 1_{(c_t \neq \sum_{i=1}^p \gamma_i c_{t-i})} \right\}. \quad (13)$$

However, (13) cannot be expressed in the form (7): the penalty in (13) induces a dependency in the calcium that spans more than two timesteps, so that the calcium at a given timestep may depend on the calcium prior to the most recent spike. As a result, (13) is computationally intractable.

Instead, we consider the  $\ell_0$  optimization problem

$$\text{minimize}_{c_1, \dots, c_T, s_2, \dots, s_T} \left\{ \frac{1}{2} \sum_{t=1}^T (y_t - c_t)^2 + \lambda \sum_{t=p+1}^T 1_{(s_t \neq 0, s_{t+1} \neq 0, \dots, s_{t+p-1} \neq 0)} \right\} \text{ subject to } s_t = c_t - \sum_{i=1}^p \gamma_i c_{t-i}, \quad (14)$$

where the indicator variable equals 1 if  $s_{t+i} \neq 0$  for some  $i$ ,  $0 \leq i \leq p-1$ . In this formulation, the calcium at a given timestep does not depend on the calcium prior to the most recent spike. Therefore, (14) is equivalent to a changepoint detection problem of the form (7) with

$$\mathcal{D}(y_{a:b}) \equiv \min \left\{ \frac{1}{2} \sum_{t=a}^b (y_t - c_t)^2 \right\} \text{ subject to } c_t = \sum_{i=1}^p \gamma_i c_{t-i}, \quad t = a + p, \dots, b.$$

Consequently, it is straightforward to develop a fast algorithm for solving (14) for the global optimum, using ideas detailed in Section 2.

### 5.3. A More Sophisticated Model for Calcium Dynamics

In a similar spirit, other models for calcium dynamics can be re-cast as  $\ell_0$  optimization problems, for which fast algorithms to solve for the global optimum can be easily developed. For instance, we could model the calcium dynamics between any pair of spikes as a difference of exponentials (Brunel and Wang, 2003; Mazzone et al., 2008; Cavallari, Panzeri and Mazzone, 2016; Volgushev, Ilin and Stevenson, 2015). This would perhaps be a better model for the data from the Allen Brain Observatory, in which increases in fluorescence due to a possible spike occur over the course of a few timesteps, rather than instantaneously (see, e.g., 62.7-63.3 seconds of Figure 5(d)).

To encode this type of calcium dynamics, consider the  $\ell_0$  optimization problem

$$\text{minimize}_{c_1, \dots, c_T, d_1, \dots, d_T} \left\{ \frac{1}{2} \sum_{t=1}^T (y_t - (c_t - d_t))^2 + \lambda \sum_{t=2}^T 1_{(c_t \neq \gamma_c c_{t-1}, d_t \neq \gamma_d d_{t-1})} \right\}. \quad (15)$$

We can recast (15) as a changepoint detection problem of the form (7), where

$$\mathcal{D}(y_{a:b}) \equiv \min \left\{ \frac{1}{2} \sum_{t=a}^b (y_t - (c_t - d_t))^2 \right\} \text{ subject to } c_t = \gamma_c c_{t-1}, d_t = \gamma_d d_{t-1}, t = a + 1, \dots, b.$$

Given  $\mathcal{D}(y_{a:b})$ ,  $\mathcal{D}(y_{a:(b+1)})$  can be updated in constant time.

## 6. Discussion

In this paper, we considered solving the seemingly intractable  $\ell_0$  optimization problem (6) corresponding to the model (2). By recasting (6) as a changepoint detection problem, we were able to derive an algorithm to solve (6) for the global optimum in expected linear time. It should be possible to develop an even more efficient algorithm for solving (6) that exploits recent algorithmic developments for changepoint detection (Johnson, 2013; Maidstone et al., 2016); we leave this as an avenue for future work.

We have shown in this paper that solving the  $\ell_0$  optimization problem (6) leads to much more accurate spike detection than solving the  $\ell_1$  optimization problem (5) proposed by Friedrich, Zhou and Paninski (2017). Indeed, this finding is intuitive: the  $\ell_1$  penalty in (5) serves as a double exponential prior on the increase in calcium at any given time point, and thereby effectively limits the amount that calcium can increase in response to a spike. By contrast, the  $\ell_0$  penalty in (6) is completely agnostic to the amount by which a spike increases the level of calcium. Consequently, it can allow for an arbitrarily large (or small) increase in fluorescence as a result of a spike.

While approximations to the solution to the  $\ell_0$  problem are possible (de Rooi and Eilers, 2011; de Rooi, Ruckebusch and Eilers, 2014; Hugelier et al., 2016; Scott and Knott, 1974; Olshen et al., 2004; Fryzlewicz et al., 2014; Friedrich, Zhou and Paninski, 2017), there is no guarantee that such approaches will yield an attractive local optimum on a given data set. In this paper, we completely bypass this concern by solving the  $\ell_0$  problem for the global optimum.

In this paper, we have focused on the empirical benefits of the  $\ell_0$  problem (6) over the  $\ell_1$  problem (5). However, it is natural to wonder whether these empirical benefits are backed by statistical theory. Conveniently, both the  $\ell_0$  and  $\ell_1$  optimization problems are very closely-related to problems that have been well-studied in the statistical literature from a theoretical standpoint. In particular, in the special case of  $\gamma = 1$ , the  $\ell_0$  problem (6) was extensively studied in Yao and Au (1989) and Boysen et al. (2009). Furthermore, when  $\gamma = 1$ , the  $\ell_1$  problem (6) is very closely-related to the *fused lasso* optimization problem,

$$\underset{c_1, \dots, c_T}{\text{minimize}} \left\{ \frac{1}{2} \sum_{t=1}^T (y_t - c_t)^2 + \lambda \sum_{t=2}^T |c_t - c_{t-1}| \right\},$$

which has also been extremely well-studied (Tibshirani et al., 2005; Mammen et al., 1997; Davies and Kovac, 2001; Rinaldo et al., 2009; Harchaoui and Lévy-Leduc, 2010; Qian and Jia, 2012; Rojas and Wahlberg, 2014; Lin et al., 2016; Dalalyan et al., 2017). However, we leave a formal theoretical analysis of the relative merits of (6) and (5), in terms of  $\ell_2$  error bounds and spike recovery properties, to future work.

Our R-language software for our proposal is available on CRAN in the package `LZeroSpikeInference`.

## Acknowledgments

We thank Michael Buice and Kyle Lepage at the Allen Institute for Brain Sciences for conversations that motivated this work. We thank Johannes Friedrich at Columbia University

for his assistance in using his software to solve the  $\ell_1$  problem (5). Sean Jewell received funding from the Natural Sciences and Engineering Research Council of Canada. This work was partially supported by NIH Grant DP5OD009145 and NSF CAREER Award DMS-1252624 to Daniela Witten.

## Appendix A: Proof of Propositions

### A.1. Proof of Proposition 1

**Proof.**

The first sentence follows by inspection. To establish the second sentence, we observe that the cost

$$\mathcal{D}(y_{a:b}) \equiv \min_{c_t = \gamma c_{t-1}, t=a+1, \dots, b} \left\{ \frac{1}{2} \sum_{t=a}^b (y_t - c_t)^2 \right\}$$

can be rewritten by direct substitution of the constraint as

$$\mathcal{D}(y_{a:b}) = \min_{c_a} \left\{ \frac{1}{2} \sum_{t=a}^b (y_t - \gamma^{t-a} c_a)^2 \right\}.$$

This is a least squares problem and is minimized at

$$\hat{c}_a = \frac{\sum_{t=a}^b y_t \gamma^{t-a}}{\sum_{t=a}^b \gamma^{2(t-a)}},$$

which implies that

$$\mathcal{D}(y_{a:b}) = \frac{1}{2} \sum_{t=a}^b (y_t - \gamma^{t-a} \hat{c}_a)^2,$$

and furthermore that for  $a < t \leq b$  the fitted values are  $\hat{c}_t = \gamma \hat{c}_{t-1}$ . Applying this argument to each segment gives the result stated in Proposition 1. □

### A.2. Proof of Proposition 2

**Proof.** The first equation follows by expanding the square for the final form of  $\mathcal{D}(y_{a:b})$  in the proof of Proposition 1. Given  $\mathcal{D}(y_{a:b})$  we can calculate  $\mathcal{D}(y_{a:(b+1)})$  in constant time by storing  $\sum_{t=a}^b \frac{y_t^2}{2}$ , and  $\sum_{t=a}^b y_t \gamma^{t-a}$  and updating each of these sums for the new data point  $y_{b+1}$ ; we use a closed form expression to calculate  $\sum_{t=a}^{b+1} \gamma^{2(t-a)}$ . With each of these quantities stored,  $\mathcal{D}(\cdot)$  and  $\mathcal{C}(\cdot)$  are updated in constant time. □

## Appendix B: Choosing $\lambda$ and $\gamma$ Through Cross-Validation

Recall that in (6), the parameters  $\lambda$  and  $\gamma$  are unknown. The nonnegative parameter  $\lambda$  controls the trade-off between the number of estimated spikes and the quality of the estimated calcium fit to the observed fluorescence. The parameter  $\gamma, 0 < \gamma < 1$ , controls the rate of exponential decay of the calcium.

In principle, we could choose both  $\lambda$  and  $\gamma$  by performing cross-validation over a two-dimensional grid of  $(\lambda, \gamma)$  values (Hastie, Tibshirani and Friedman, 2009). However, this approach would be very computationally intensive, because a very fine grid of values for  $\gamma$  would need to be used.

Therefore, instead of performing cross-validation on a two-dimensional grid, we perform cross-validation over a one-dimensional grid of  $\lambda$  values. For each value of  $\lambda$  in this grid, we solve (7) on a training set using a candidate value for  $\gamma$ . Given the resulting set of changepoints, we solve a one-dimensional constrained optimization problem for  $\gamma$ . We then refit (7) with the optimized value of  $\gamma$ , and then evaluate the mean squared error (MSE) on a hold-out set. Details are provided in Algorithm 3. Note that in the final output of the algorithm, we take the square root of the optimal value of  $\gamma$  in order to address the fact that the cross-validation scheme makes use of training and test sets consisting of alternately-spaced timesteps.

---

**Algorithm 3:** A Cross-Validation Scheme for Choosing  $\lambda$  and  $\gamma$  in (6)

---

**Initialize:** Candidate tuning parameter values  $\lambda_1, \dots, \lambda_M$ ; an initial guess  $\hat{\gamma}$  for the rate of exponential decay; a matrix  $\text{cvMSE} \in \mathbb{R}^{M \times 2}$  to store the cross-validated MSEs; and a matrix  $\Gamma \in \mathbb{R}^{M \times 2}$  to store the optimal values of  $\gamma$ .

1 **foreach** *fold in 1, 2* **do**

2     Assign odd timesteps to the training set and even timesteps to the test set for the first fold, and vice-versa for the second fold. Note that  $\text{card}(y^{\text{train}}) = \text{card}(y^{\text{test}}) = T/2$ .

3     **foreach**  $m = 1, \dots, M$  **do**

4         Solve (7) on the training set  $y^{\text{train}}$  with tuning parameter values  $\lambda_m$  and  $\hat{\gamma}$ , in order to obtain an initial estimate of the changepoints  $\tau_1, \dots, \tau_k$ . Set  $\tau_0 = 0$  and  $\tau_{k+1} = T/2$ .

5         Given the changepoints  $\tau_1, \dots, \tau_k$ , compute the value of  $\gamma$  that minimizes the training set MSE,

$$\hat{\gamma} = \underset{\gamma}{\operatorname{argmin}} \left\{ \sum_{j=0}^k \mathcal{D} \left( y_{(\tau_j+1):\tau_{j+1}}^{\text{train}} \right) \right\} = \underset{\gamma}{\operatorname{argmin}} \left\{ \sum_{j=0}^k \min_{c_t = \gamma c_{t-1}, t = \tau_j+2, \dots, \tau_{j+1}} \left\{ \frac{1}{2} \sum_{t=\tau_j+1}^{\tau_{j+1}} (y_t^{\text{train}} - c_t)^2 \right\} \right\}.$$

This can be done via numerical optimization. Set  $\Gamma_{m,\text{fold}} = \hat{\gamma}$ .

6         Solve (7) on the training set  $y^{\text{train}}$  with tuning parameter values  $\lambda_m$  and  $\hat{\gamma}$  in order to obtain fitted values  $\hat{c}^{\text{train}}$ .

7         Average adjacent fitted values in order to obtain predictions on the test set  $y^{\text{test}}$ ,

$$\hat{c}^{\text{test}} = \frac{\hat{c}_{1:(T/2-1)}^{\text{train}} + \hat{c}_{2:(T/2)}^{\text{train}}}{2}.$$

8         Calculate and store the test set MSE,

$$\text{cvMSE}_{m,\text{fold}} = \frac{2}{T} \sum_{t=1}^{T/2} (y_t^{\text{test}} - \hat{c}_t^{\text{test}})^2.$$

9         **end**

10 **end**

11 Average the test set MSE and  $\Gamma$  over folds,

$$\overline{\text{cvMSE}}_m = \frac{1}{2} (\text{cvMSE}_{m,1} + \text{cvMSE}_{m,2}), \quad \bar{\Gamma}_m = \frac{1}{2} (\Gamma_{m,1} + \Gamma_{m,2}), \quad \text{for } m = 1, \dots, M.$$

12 Calculate  $\hat{m} = \underset{m}{\operatorname{argmin}} \{ \overline{\text{cvMSE}}_m \}$ .

13 Calculate the standard error of the test set MSE over folds,

$$\text{se}(\text{cvMSE})_m = \sqrt{\frac{(\text{cvMSE}_{m,1} - \overline{\text{cvMSE}}_m)^2 + (\text{cvMSE}_{m,2} - \overline{\text{cvMSE}}_m)^2}{2}}, \quad \text{for } m = 1, \dots, M.$$

14 Calculate

$$m^* = \max \{ m : \overline{\text{cvMSE}}_m \leq \overline{\text{cvMSE}}_{\hat{m}} + \text{se}(\text{cvMSE})_{\hat{m}} \}.$$

**Output :** The values  $(\lambda_{\hat{m}}, \sqrt{\bar{\Gamma}_{\hat{m}}})$  that minimize the cross-validated MSE, and the values  $(\lambda_{m^*}, \sqrt{\bar{\Gamma}_{m^*}})$  selected based on the one-standard-error rule (Hastie, Tibshirani and Friedman, 2009).

---

## Appendix C: A Comparison to Two Additional Approaches

In this section, we explore two additional approaches for recovering spikes:

1. Post-thresholding the estimated spikes  $\hat{s}_2, \dots, \hat{s}_T$  that result from (5), in order to eliminate very small spikes; and
2. Approximating the solution to a non-convex problem using a greedy algorithm proposed by Friedrich, Zhou and Paninski (2017).

We investigate the performances of these two approaches on a subset of the Chen et al. (2013) data presented in Section 4.1.

### C.1. Post-Thresholding the Solution to (5)

We see from Figure 1(d) that much of the poor performance of the  $\ell_1$  problem (5) is due to estimation of many “small” spikes: i.e.  $\hat{s}_t$  is near zero, but not exactly equal to zero, for many timesteps. This suggests that we could improve the results of the  $\ell_1$  problem by thresholding the solution  $\hat{s}_2, \dots, \hat{s}_T$  by a quantity  $L$ , in order to yield the thresholded solution  $\tilde{s}_t = \hat{s}_t 1_{(\hat{s}_t \geq L)}$  for  $t = 2, \dots, T$ .

Figure 6 illustrates the behavior of this post-thresholding method for different values of the threshold  $L$ , with  $\lambda = 1$  and  $\gamma = 0.9864405$ . When  $L = 0.1$  in panel (b), the post-thresholding solution is very close to the ground truth between 10 – 30s. However, the zoomed-in view in panel (e) indicates that when  $L = 0.1$ , the post-thresholding approach estimates too many spikes between 6 – 8s. Increasing  $L$  to 0.12, in panels (c) and (f), induces additional sparsity, but results in several missed spikes between 20 – 25s.

Overall, while post-thresholding the solution to the  $\ell_1$  problem (5) clearly improves its performance, the post-thresholded solution does not perform as well as the solution to the  $\ell_0$  problem (6). Furthermore, in practice, application of the post-thresholding procedure is complicated by the presence of an additional tuning parameter,  $L$ .

### C.2. A Greedy Approach for Approximating the Solution to a Non-Convex Problem

Friedrich, Zhou and Paninski (2017) consider a variant of the optimization problem (5),

$$\underset{c_1, \dots, c_T, s_2, \dots, s_T}{\text{minimize}} \left\{ \frac{1}{2} \sum_{t=1}^T (y_t - c_t)^2 \right\} \text{ subject to } s_t = c_t - \gamma c_{t-1} \geq s_{\min} \text{ or } s_t = 0, \quad (16)$$

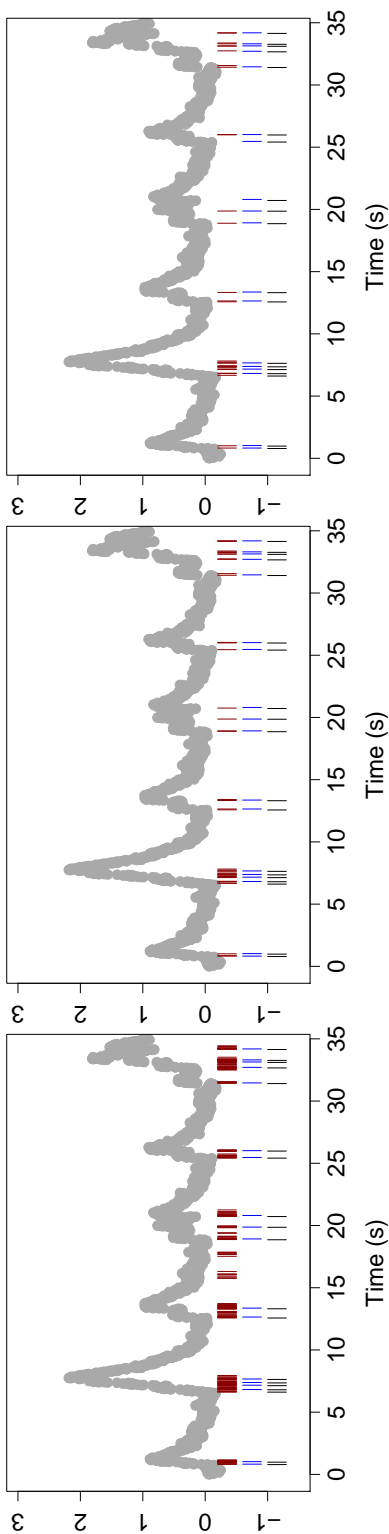
obtained from (5) by setting  $\lambda = 0$ , and changing the convex positivity constraint to the non-convex constraint that  $s_t$  lies within a non-convex set. Like (6), (16) is non-convex. Friedrich, Zhou and Paninski (2017) do not attempt to solve (16) for the global optimum; instead, they provide a heuristic modification to their algorithm for solving (6), which is intended to approximate the solution to (16).

Figure 7 illustrates the behavior of this approximate algorithm when applied to the same data as in Figure 6. We set  $\gamma = 0.9864405$ , and considered three values of  $s_{\min}$ . When

$s_{min} = 10^{-8}$  and  $s_{min} = 0.1$ , in panels (a) to (b), too many spikes are estimated. But when  $s_{min} = 0.3$ , in panel (c), the solution to (16) is very similar to the solution of (6) with  $\lambda = 0.6$ . Both almost perfectly recover the ground truth spikes. Therefore, in this example, the approximate algorithm of Friedrich, Zhou and Paninski (2017) for solving (16) performs quite well.

However, (16) is a non-convex problem, and the approximate algorithm of Friedrich, Zhou and Paninski (2017) is not guaranteed to find the global minimum. In fact, we can see that on the data shown in Figure 7, this approximate algorithm does not find the global optimum. When applied with  $s_{min} = 0.3$ , the approximate algorithm yields an objective value of 8.57. By contrast, our algorithm for solving (6) yields a solution that is feasible for (16), and which results in a value of 7.86 for the objective of (16). We emphasize that this is quite remarkable: even though the algorithm proposed in Section 2 solves (6) and not (16), *it nonetheless yields a solution that is closer to the global optimum of (16) than does the approximate algorithm of Friedrich, Zhou and Paninski (2017), which is intended to solve (16).*

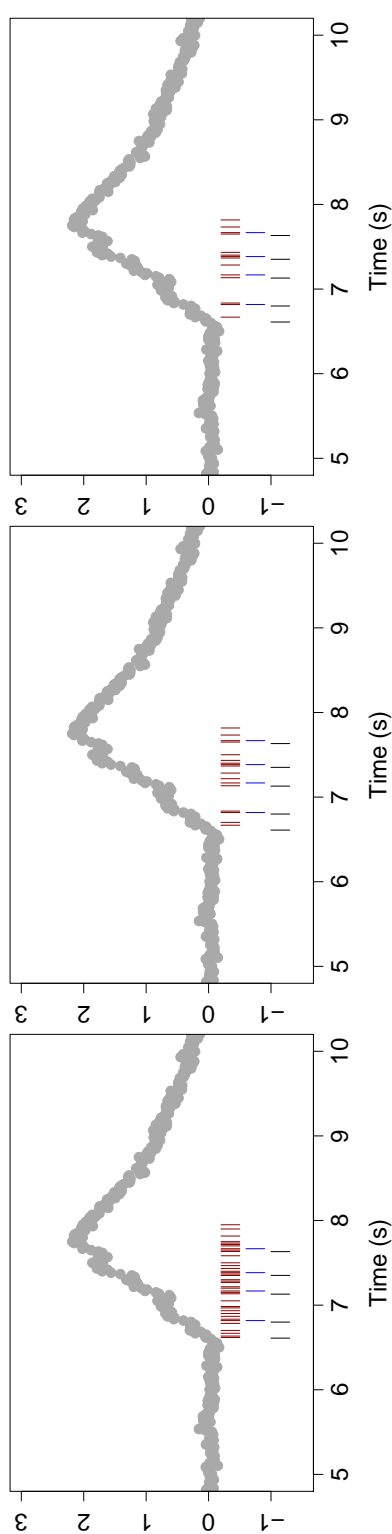
In many cases, the greedy algorithm of Friedrich, Zhou and Paninski (2017) for solving (16) might yield good results that are near the global optimum of (16), and potentially even near the global optimum of (6). However, there is no guarantee that this algorithm will yield a “good” local optimum on any given data set. By contrast, in this paper we have proposed an elegant and efficient algorithm for exactly solving the  $\ell_0$  problem (6).



(a)  $L = 10^{-8}$ .

(b)  $L = 0.1$

(c)  $L = 0.12$



(d) Zoomed  $L = 10^{-8}$

(e) Zoomed  $L = 0.1$

(f) Zoomed  $L = 0.12$

Fig 6: Spike detection for cell 2002 of the [Chen et al. \(2013\)](#) data. In each panel, the observed fluorescence ( $\bullet$ ) and true spikes ( $\text{---}$ ) are displayed. Estimated spikes  $\tilde{s}_t$  from post-thresholding are shown in ( $\text{---}$ ), and the estimated spikes from the  $\ell_0$  problem (6) with  $\lambda = 0.6$  are shown in ( $\text{---}$ ). Times  $0s - 35s$  are shown in the top row; the second row zooms into time  $5s - 10s$  in order to illustrate the behavior around a large increase in calcium concentration. Columns correspond to different values of the threshold  $L$ .

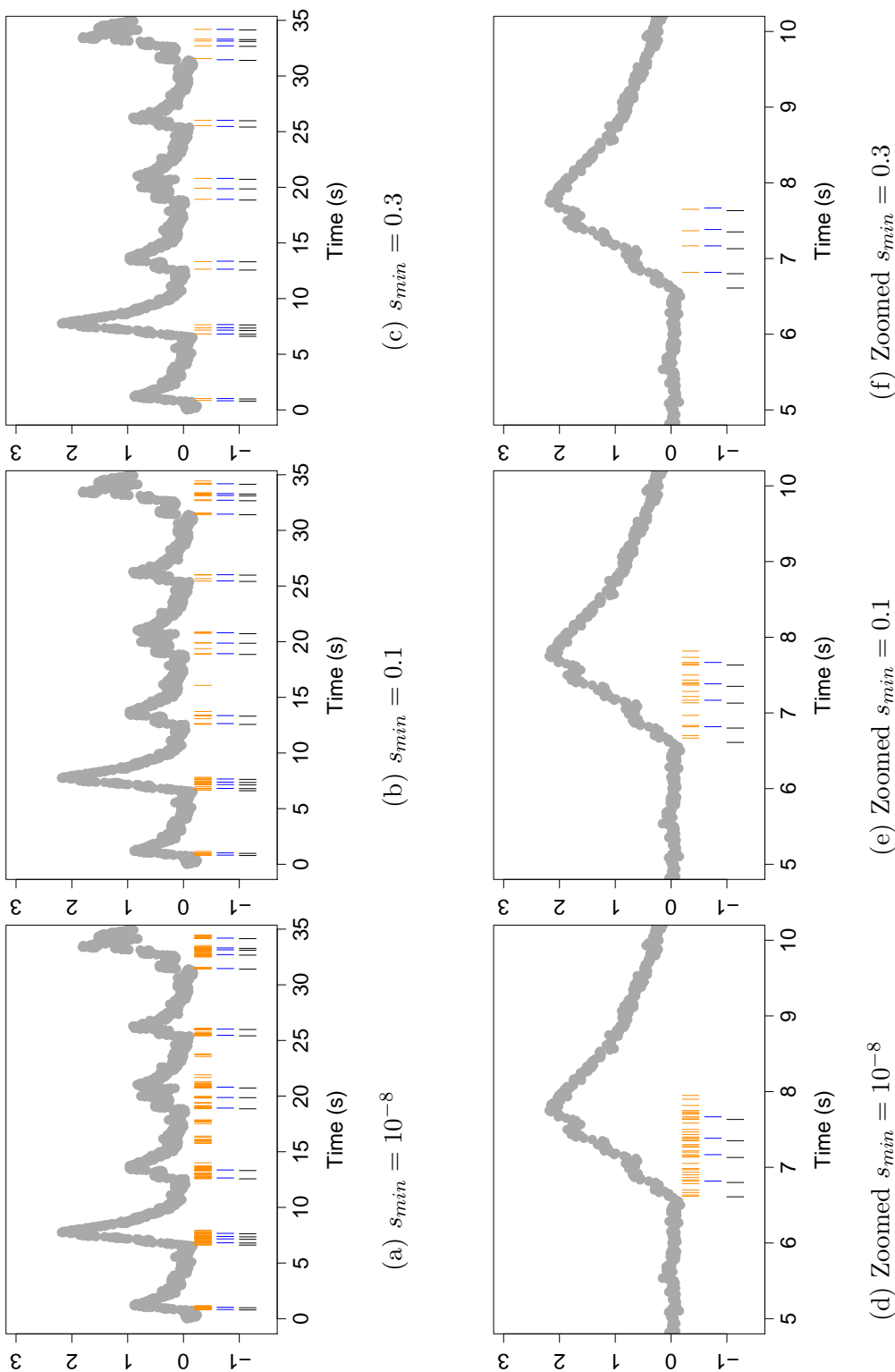


Fig 7: Spike detection for cell 2002 of the [Chen et al. \(2013\)](#) data. In each panel, the observed fluorescence ( $\bullet$ ) and true spikes ( $\text{—}$ ) are displayed. Estimated spikes from problem (16) are shown in ( $\text{—}$ ), and the estimated spikes from the  $\ell_0$  problem (6) with  $\lambda = 0.6$  are shown in ( $\text{—}$ ). Times  $0s - 35s$  are shown in the top row; the second row zooms in on times  $5s - 10s$  to illustrate behavior around a large increase in calcium concentration. Columns correspond to different values of  $s_{min}$ .

## References

- AHRENS, M. B., ORGER, M. B., ROBSON, D. N., LI, J. M. and KELLER, P. J. (2013). Whole-brain functional imaging at cellular resolution using light-sheet microscopy. *Nature Methods* **10** 413–420.
- AUE, A. and HORVÁTH, L. (2013). Structural breaks in time series. *Journal of Time Series Analysis* **34** 1–16.
- AUGER, I. E. and LAWRENCE, C. E. (1989). Algorithms for the optimal identification of segment neighborhoods. *Bulletin of Mathematical Biology* **51** 39–54.
- BIEN, J. and WITTEN, D. (2016). *Penalized Estimation in Complex Models, in Handbook of Big Data* 285–303. CRC Press.
- BOYD, S. and VANDENBERGHE, L. (2004). *Convex Optimization*. Cambridge University Press.
- BOYSEN, L., KEMPE, A., LIEBSCHER, V., MUNK, A. and WITTICH, O. (2009). Consistencies and rates of convergence of jump-penalized least squares estimators. *The Annals of Statistics* 157–183.
- BRAUN, J. V. and MULLER, H.-G. (1998). Statistical methods for DNA sequence segmentation. *Statistical Science* 142–162.
- BRUNEL, N. and WANG, X.-J. (2003). What determines the frequency of fast network oscillations with irregular neural discharges? I. Synaptic dynamics and excitation-inhibition balance. *Journal of Neurophysiology* **90** 415–430.
- CAVALLARI, S., PANZERI, S. and MAZZONI, A. (2016). Comparison of the dynamics of neural interactions between current-based and conductance-based integrate-and-fire recurrent networks. *Frontiers in Neural Circuits* **8**.
- CHEN, T.-W., WARDILL, T. J., SUN, Y., PULVER, S. R., RENNINGER, S. L., BAOHAN, A., SCHREITER, E. R., KERR, R. A., ORGER, M. B., JAYARAMAN, V. et al. (2013). Ultrasensitive fluorescent proteins for imaging neuronal activity. *Nature* **499** 295–300.
- DALALYAN, A. S., HEBIRI, M., LEDERER, J. et al. (2017). On the prediction performance of the Lasso. *Bernoulli* **23** 552–581.
- DAVIES, P. L. and KOVAC, A. (2001). Local extremes, runs, strings and multiresolution. *Annals of Statistics* 1–48.
- DAVIS, R. A., LEE, T. C. M. and RODRIGUEZ-YAM, G. A. (2006). Structural break estimation for nonstationary time series models. *Journal of the American Statistical Association* **101** 223–239.
- DE ROOI, J. and EILERS, P. (2011). Deconvolution of pulse trains with the L 0 penalty. *Analytica chimica acta* **705** 218–226.
- DE ROOI, J. J., RUCKEBUSCH, C. and EILERS, P. H. (2014). Sparse deconvolution in one and two dimensions: Applications in endocrinology and single-molecule fluorescence imaging. *Analytical chemistry* **86** 6291–6298.
- DENEUX, T., KASZAS, A., SZALAY, G., KATONA, G., LAKNER, T., GRINVALD, A., RÓZSA, B. and VANZETTA, I. (2016). Accurate spike estimation from noisy calcium signals for ultrafast three-dimensional imaging of large neuronal populations in vivo. *Nature Communications* **7**.

- DOMBECK, D. A., KHABBAZ, A. N., COLLMAN, F., ADELMAN, T. L. and TANK, D. W. (2007). Imaging large-scale neural activity with cellular resolution in awake, mobile mice. *Neuron* **56** 43–57.
- ALLEN INSTITUTE FOR BRAIN SCIENCES (2016). Stimulus Set and Response Analysis Technical Report, Allen Institute.
- FRIEDRICH, J. and PANINSKI, L. (2016). Fast active set methods for online spike inference from calcium imaging. In *Advances In Neural Information Processing Systems* 1984–1992.
- FRIEDRICH, J., ZHOU, P. and PANINSKI, L. (2017). Fast online deconvolution of calcium imaging data. *PLoS Comput Biol* **13**.
- FRYZLEWICZ, P. et al. (2014). Wild binary segmentation for multiple change-point detection. *The Annals of Statistics* **42** 2243–2281.
- GREWE, B. F., LANGER, D., KASPER, H., KAMPA, B. M. and HELMCHEN, F. (2010). High-speed in vivo calcium imaging reveals neuronal network activity with near-millisecond precision. *Nature Methods* **7** 399–405.
- HARCHAOU, Z. and LÉVY-LEDUC, C. (2010). Multiple change-point estimation with a total variation penalty. *Journal of the American Statistical Association* **105** 1480–1493.
- HASTIE, T., TIBSHIRANI, R. and FRIEDMAN, J. (2009). *The Elements of Statistical Learning; Data Mining, Inference and Prediction*. Springer Verlag, New York.
- HASTIE, T., TIBSHIRANI, R. and WAINWRIGHT, M. (2015). *Statistical Learning with Sparsity*. CRC Press.
- HAWRYLYCZ, M., ANASTASSIOU, C., ARKHIPOV, A., BERG, J., BUICE, M., CAIN, N., GOUWENS, N. W., GRATIY, S., IYER, R., LEE, J. H. et al. (2016). Inferring cortical function in the mouse visual system through large-scale systems neuroscience. *Proceedings of the National Academy of Sciences* **113** 7337–7344.
- HOLEKAMP, T. F., TURAGA, D. and HOLY, T. E. (2008). Fast three-dimensional fluorescence imaging of activity in neural populations by objective-coupled planar illumination microscopy. *Neuron* **57** 661–672.
- HUGELIER, S., DE ROOI, J. J., BERNEX, R., DUWÉ, S., DEVOS, O., SLIWA, M., DEDECKER, P., EILERS, P. H. and RUCKEBUSCH, C. (2016). Sparse deconvolution of high-density super-resolution images. *Scientific reports* **6**.
- JACKSON, B., SCARGLE, J. D., BARNES, D., ARABHI, S., ALT, A., GIOUMOUSIS, P., GWIN, E., SANGTRAKULCHAROEN, P., TAN, L. and TSAI, T. T. (2005). An algorithm for optimal partitioning of data on an interval. *IEEE Signal Processing Letters* **12** 105–108.
- JOHNSON, N. A. (2013). A dynamic programming algorithm for the fused lasso and  $\ell_0$ -segmentation. *Journal of Computational and Graphical Statistics* **22** 246–260.
- KILLICK, R., FEARNHEAD, P. and ECKLEY, I. A. (2012). Optimal detection of change-points with a linear computational cost. *Journal of the American Statistical Association* **107** 1590–1598.
- LEE, C.-B. (1995). Estimating the number of change points in a sequence of independent normal random variables. *Statistics & Probability Letters* **25** 241–248.
- LIN, K., SHARPBACK, J., RINALDO, A. and TIBSHIRANI, R. J. (2016). Approximate Recovery in Changepoint Problems, from  $\ell_2$  Estimation Error Rates. *arXiv preprint arXiv:1606.06746*.
- MAIDSTONE, R., HOCKING, T., RIGAILL, G. and FEARNHEAD, P. (2016). On optimal

- multiple changepoint algorithms for large data. *Statistics and Computing*.
- MAMMEN, E., VAN DE GEER, S. et al. (1997). Locally adaptive regression splines. *The Annals of Statistics* **25** 387–413.
- MAZZONI, A., PANZERI, S., LOGOTHETIS, N. K. and BRUNEL, N. (2008). Encoding of naturalistic stimuli by local field potential spectra in networks of excitatory and inhibitory neurons. *PLoS Comput Biol* **4** e1000239.
- OLSHEN, A. B., VENKATRAMAN, E., LUCITO, R. and WIGLER, M. (2004). Circular binary segmentation for the analysis of array-based DNA copy number data. *Biostatistics* **5** 557–572.
- PNEVMATIKAKIS, E. A., MEREL, J., PAKMAN, A. and PANINSKI, L. (2013). Bayesian spike inference from calcium imaging data. In *Signals, Systems and Computers, 2013 Asilomar Conference on* 349–353. IEEE.
- PNEVMATIKAKIS, E. A., SOUDRY, D., GAO, Y., MACHADO, T. A., MEREL, J., PFAU, D., REARDON, T., MU, Y., LACEFIELD, C., YANG, W. et al. (2016). Simultaneous denoising, deconvolution, and demixing of calcium imaging data. *Neuron* **89** 285–299.
- PREVEDEL, R., YOON, Y.-G., HOFFMANN, M., PAK, N., WETZSTEIN, G., KATO, S., SCHRÖDEL, T., RASKAR, R., ZIMMER, M., BOYDEN, E. S. et al. (2014). Simultaneous whole-animal 3D imaging of neuronal activity using light-field microscopy. *Nature Methods* **11** 727–730.
- GENIE PROJECT (2015). Simultaneous imaging and loose-seal cell-attached electrical recordings from neurons expressing a variety of genetically encoded calcium indicators. *CRCNS.org*.
- QIAN, J. and JIA, J. (2012). On pattern recovery of the fused lasso. *arXiv preprint arXiv:1211.5194*.
- RINALDO, A. et al. (2009). Properties and refinements of the fused lasso. *The Annals of Statistics* **37** 2922–2952.
- ROJAS, C. R. and WAHLBERG, B. (2014). On change point detection using the fused lasso method. *arXiv preprint arXiv:1401.5408*.
- SASAKI, T., TAKAHASHI, N., MATSUKI, N. and IKEGAYA, Y. (2008). Fast and accurate detection of action potentials from somatic calcium fluctuations. *Journal of Neurophysiology* **100** 1668–1676.
- SCOTT, A. J. and KNOTT, M. (1974). A cluster analysis method for grouping means in the analysis of variance. *Biometrics* 507–512.
- THEIS, L., BERENS, P., FROUDARAKIS, E., REIMER, J., ROSÓN, M. R., BADEN, T., EULER, T., TOLIAS, A. S. and BETHGE, M. (2016). Benchmarking spike rate inference in population calcium imaging. *Neuron* **90** 471–482.
- TIBSHIRANI, R. (1996). Regression shrinkage and selection via the lasso. *J. Royal. Statist. Soc. B.* **58** 267–288.
- TIBSHIRANI, R., SAUNDERS, M., ROSSET, S., ZHU, J. and KNIGHT, K. (2005). Sparsity and smoothness via the fused lasso. *J. Royal. Statist. Soc. B.* **67** 91–108.
- VOGELSTEIN, J. T., WATSON, B. O., PACKER, A. M., YUSTE, R., JEDYNAK, B. and PANINSKI, L. (2009). Spike inference from calcium imaging using sequential Monte Carlo methods. *Biophysical Journal* **97** 636–655.
- VOGELSTEIN, J. T., PACKER, A. M., MACHADO, T. A., SIPPY, T., BABADI, B.,

- YUSTE, R. and PANINSKI, L. (2010). Fast nonnegative deconvolution for spike train inference from population calcium imaging. *Journal of Neurophysiology* **104** 3691–3704.
- VOLGUSHEV, M., ILIN, V. and STEVENSON, I. H. (2015). Identifying and tracking simulated synaptic inputs from neuronal firing: insights from in vitro experiments. *PLOS Comput Biol* **11** e1004167.
- YAKSI, E. and FRIEDRICH, R. W. (2006). Reconstruction of firing rate changes across neuronal populations by temporally deconvolved Ca<sup>2+</sup> imaging. *Nature Methods* **3** 377–383.
- YAO, Y.-C. (1988). Estimating the number of change-points via Schwarz’ criterion. *Statistics & Probability Letters* **6** 181–189.
- YAO, Y.-C. and AU, S.-T. (1989). Least-squares estimation of a step function. *Sankhyā: The Indian Journal of Statistics, Series A* 370–381.
- ZOU, H. (2006). The adaptive lasso and its oracle properties. *Journal of the American Statistical Association* **101** 1418–1429.